

# GROWTH OF EARLY SUPERMASSIVE BLACK HOLES AND THE HIGH-REDSHIFT EDDINGTON RATIO DISTRIBUTION

C. DEGRAF,<sup>1</sup> T. DI MATTEO,<sup>1</sup> N. KHANDAI,<sup>1</sup> R. CROFT<sup>1</sup>

*Draft version January 27, 2012*

## ABSTRACT

Using a new large-scale ( $\sim 0.75 Gpc$ )<sup>3</sup> hydrodynamic cosmological simulation we investigate the growth rate of supermassive black holes in the early universe ( $z \gtrsim 4.75$ ). Remarkably we find a clear peak in the typical Eddington ratio ( $\lambda$ ) at black hole masses of  $4 - 8 \times 10^7 M_\odot$  (typically found in halos of  $\sim 7 \times 10^{11} - 1 \times 10^{12} M_\odot$ ), independent of redshift and indicative that most of BH growth occurs in the cold-flow dominated regime. Black hole growth is by and large regulated by the evolution of gas density. The typical Eddington ratio at a given mass scales simply as cosmological density  $(1+z)^3$  and the peak is caused by the competition between increased gas density available in more massive hosts, and a decrease due to strong AGN feedback that deprives the black hole of sufficient gas to fuel further rapid growth in the high mass end. In addition to evolution in the mean Eddington ratio, we show that the distribution of  $\lambda$  among both mass-selected and luminosity-selected samples is approximately log-normal. We combine these findings into a single log-normal fitting formula for the distribution of Eddington ratios as a function of  $(M_{BH}, z)$ . This formula can be used in analytic and semi-analytic models for evolving black hole populations, predicting black hole masses of observed quasars, and, in conjunction with the observed distribution of Eddington ratios, can be used to constrain the black hole mass function.

*Subject headings:* quasars: general — galaxies: active — black hole physics — methods: numerical — galaxies: evolution

## 1. INTRODUCTION

It has been well established that supermassive black holes are present in the center of most galaxies (Kormendy & Richstone 1995), and that they are correlated with the properties of their hosts (Magorrian et al. 1998; Ferrarese & Merritt 2000; Gebhardt et al. 2000; Tremaine et al. 2002; Graham & Driver 2007). These correlations provide strong evidence that the growth of a black hole and the evolution of its host galaxy directly influence one another, such that black hole growth is a important aspect of understanding galactic evolution and vice versa.

In general, the link between black hole and galactic evolution is attributed to some form of quasar feedback (Barkett & Silk 2001; Sazonov et al. 2004; Springel et al. 2005b; Churazov et al. 2005; Di Matteo et al. 2005; Bower et al. 2006; Ciotti & Ostriker 2007; Sijacki et al. 2007; Hopkins et al. 2007b) which can result in the self-regulation of the growth of the black hole (see, e.g. Di Matteo et al. 2005). In this model we would expect black holes to grow rapidly during their early lifetime (i.e. while at low mass), until some point at which the black hole feedback begins to significantly affect its environment, resulting in a noticeable decline in growth rate. This effect has been observed in individual black hole histories, but such investigations (see, e.g. Sijacki et al. 2009; Di Matteo et al. 2011) have tended to focus on the largest mass black holes, primarily to explain how black holes could grow rapidly enough to produce the extremely large masses ( $\sim 10^9 M_\odot$  by  $z \sim 6$ ) found in observations by the Sloan Digital Sky Survey (e.g. Fan et al.

2006; Jiang et al. 2009). In this paper we take advantage of a new, very large simulation to investigate the growth histories of early universe black holes across a wide range of masses, probing both the mean and the distribution of growth rates for black holes across a wide range of masses and luminosities, and provide fits for these distributions.

## 2. METHOD

In this paper we use a new cosmological hydrodynamic simulation of a  $533 h^{-1}$  Mpc box specifically intended for high-redshift investigations. The simulation uses the massively parallel cosmological TreePM-SPH code P-GADGET (an updated version of GADGET-2, see Springel 2005) incorporating a multi-phase ISM model with star formation (Springel & Hernquist 2003) and black hole accretion and feedback (Springel et al. 2005a; Di Matteo et al. 2005), has a gravitational softening length of  $5 h^{-1}$  kpc and mass resolution of  $2.8 \times 10^8 M_\odot$  for dark matter and  $5.7 \times 10^7 M_\odot$  for gas.

Within the simulation, black holes are modeled as collisionless sink particles which form in newly emerging and resolved dark matter halos. These halos are found by calling a friends of friends group finder at regular intervals (in time intervals spaced by  $\Delta \log a = \log 1.25$ ). Any group above a threshold mass of  $5 \times 10^{10} h^{-1} M_\odot$  not already containing a black hole is provided one by converting its densest particle to a sink particle with a seed mass of  $M_{BH,seed} = 5 \times 10^5 h^{-1} M_\odot$ . This seeding prescription is chosen to reasonably match the expected formation of supermassive black holes by gas directly collapsing to BHs with  $M_{BH} \sim M_{seed}$  (e.g. Bromm & Loeb 2003; Begelman et al. 2006) or by PopIII stars collapsing to  $\sim 10^2 M_\odot$  BHs at  $z \sim 30$  (Bromm & Larson 2004; Yoshida et al. 2006) followed by sufficient expo-

<sup>1</sup> McWilliams Center for Cosmology, Carnegie Mellon University, 5000 Forbes Avenue, Pittsburgh, PA 15213, USA

ponential growth to reach  $M_{\text{seed}}$  by the time the host halo reaches  $\sim 10^{10} M_{\odot}$ . Following insertion, BHs grow in mass by accretion of surrounding gas and by merging with other black holes. Gas is accreted according to  $\dot{M}_{\text{BH}} = \alpha \frac{4\pi G^2 M_{\text{BH}}^2 \rho_{\text{BH}}}{(c_s^2 + v^2)^{3/2}}$ , where  $\rho_{\text{BH}}$  is the local gas density (determined from the gas particles within the black hole kernel),  $c_s$  is the local sound speed,  $v$  is the velocity of the BH relative to the surrounding gas, and  $\alpha$  is introduced to correct for the reduction of the gas density close to the BH due to our effective sub-resolution model for the ISM. To allow for the initial rapid BH growth necessary to produce sufficiently massive BHs at early time ( $\sim 10^9 M_{\odot}$  by  $z \sim 6$ ) we allow for mildly super-Eddington accretion, but limit it to a maximum of  $3 \times \dot{M}_{\text{Edd}}$  to prevent artificially high values.

The BH is assumed to radiate with a bolometric luminosity proportional to the accretion rate,  $L = \eta \dot{M}_{\text{BH}} c^2$  (Shakura & Sunyaev 1973), where the radiative efficiency  $\eta$  is fixed to 0.1 throughout the simulation and our analysis. To model the expected coupling between the liberated radiation and the surrounding gas, 5 per cent of the luminosity is isotropically deposited to the local black hole kernel as thermal energy. The 5 per cent value for the coupling factor is based on galaxy merger simulations such that the normalization of the  $M_{\text{BH}} - \sigma$  relation is reproduced (Di Matteo et al. 2005).

The second mode of black hole growth is through mergers which occur when dark matter halos merge into a single halo, such that their black holes fall toward the center of the new halo, eventually merging with one another. In cosmological volumes, it is not possible to directly model the physics of the infalling BHs at the smallest scales, so a sub-resolution model is used. Since the mergers typically occur at the center of a galaxy (i.e. a gas-rich environment), we assume the final coalescence will be rapid (e.g. Mayer et al. 2007), so we merge the BHs once they are within the spatial resolution of the simulation. However, to prevent merging of BHs which are rapidly passing one another, mergers are prevented if the BHs' velocity relative to one another is too high (comparable to the local sound speed).

The model used for black hole creation, accretion and feedback has been investigated and discussed in Sijacki et al. (2007); Di Matteo et al. (2008); Colberg & di Matteo (2008); Sijacki et al. (2009); DeGraf et al. (2010); Degraf et al. (2011), finding it does a good job reproducing the  $M_{\text{BH}} - \sigma$  relation, the total black hole mass density (Di Matteo et al. 2008), the QLF (DeGraf et al. 2010), and the expected black hole clustering behavior (Degraf et al. 2011). This simple model thus appears to model the growth, activity, and evolution of supermassive black holes in a cosmological context surprisingly well (though the detailed treatment of the accretion physics is infeasible for cosmological scale simulations). We also note that Booth & Schaye (2009) and Johansson et al. (2008) have adopted a very similar model, and have independently investigated the parameter space of the reference model of Di Matteo et al. (2008), as well as varying some of the underlying prescriptions. In addition, this simulation has previously been used to investigate the growth of the first very massive black holes (Di Matteo et al. 2011), statistical properties of quasars (DeGraf et al. 2011),

and large scale high-resolution imaging (Feng et al. 2011). For further details on the simulation methods and convergence studies done for similar simulations, see Di Matteo et al. (2008).

Because the simulation saves the complete set of black hole properties (mass, accretion rate, position, local gas density, sound speed, velocity, and BH velocity relative to local gas) for each BH at every timestep, the black hole output for such a large simulation is prohibitively difficult to analyze using previous techniques. For this reason, Lopez et al. (2011) developed a relational database management system specifically for this simulation. A similar strategy has also been followed in the analysis of the Millenium simulation (Lemson & Virgo Consortium 2006). In addition to providing a substantially more efficient query system for extracting information, this database is significantly more flexible than traditional approaches. For a complete summary of the database format and its efficiency, please see Lopez et al. (2011).

### 3. RESULTS

#### 3.1. Typical Black Hole Growth Rates

To quantify the growth rate of black holes, we use the mean Eddington ratio ( $\lambda = \frac{\dot{M}_{\text{BH}}}{\dot{M}_{\text{Edd}}}$ ) which we calculate for each black hole over a finite time interval. Because we have the complete BH growth history, we are able to compute this quantity based solely on the gas accretion, and neglect any mass gained through black hole mergers (though we find the mass gained by mergers to be small enough to have a negligible effect on our results). In Figure 1 we plot  $\langle \lambda \rangle / (1+z)^3$  as a function of  $M_{\text{BH,initial}}$  for several redshift ranges. We plot  $\langle \lambda \rangle / (1+z)^3$  rather than  $\langle \lambda \rangle$  for two reasons: First, to show that the dependence of  $\langle \lambda \rangle$  on  $M_{\text{BH}}$  is independent of redshift (at least for  $z \geq 4.75$ ), and second to show that  $\langle \lambda \rangle \propto (1+z)^3$ .

Regardless of redshift considered, we find similar behavior for Eddington ratio with respect to mass: more massive black holes grow faster than low mass black holes up to a peak growth rate at  $M_{\text{BH}} \sim 4 - 8 \times 10^7 M_{\odot}$ , while the black holes above this characteristic mass grow more slowly. Thus black holes grow fastest (relative to their current mass) while at intermediate masses, and grow slower at higher mass.

We find this peak in the Eddington ratio to be caused by the change in the local gas density available for fueling BH growth. We plot the evolution in local gas density ( $\rho_{\text{BH}}$ , the density of gas contributing to  $\dot{M}_{\text{BH}}$ ) with mass in Figure 1, showing a clear peak at  $\sim 5 \times 10^7 M_{\odot}$ . We note that neither the sound speed nor the BH velocity (the other factors in the calculation of  $\dot{M}_{\text{BH}}$ ) exhibit a peak with respect to  $M_{\text{BH}}$ , confirming that the peak Eddington ratio is caused by the evolution in the local gas density. To show how the gas density evolves, in Figure 2 we show the gas density profiles around BHs below the Eddington ratio peak ( $\sim 10^7 M_{\odot}$  - blue), at the peak ( $\sim 5 \times 10^7 M_{\odot}$  - green), and above the peak ( $\sim 4 \times 10^8 M_{\odot}$  - red), each averaged across 100 BHs. In general we find the gas density profile to grow with  $M_{\text{BH}}$  until  $M_{\text{BH}} \sim 5 \times 10^7 M_{\odot}$  (as expected for BHs found in more massive halos). Above  $\sim 5 \times 10^7 M_{\odot}$  the gas density away from the BH continues to grow, but the innermost density is suppressed, with the suppression growing with

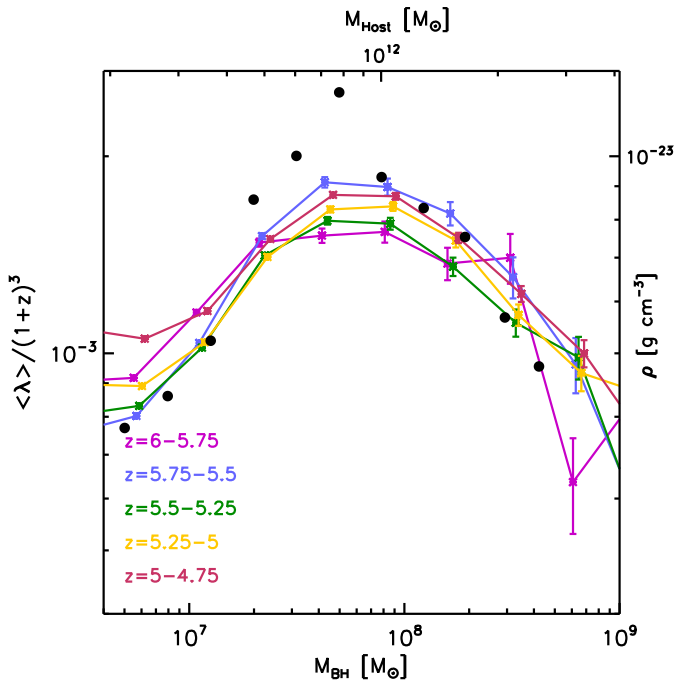


FIG. 1.— *Colored lines*: The mean Eddington ratio ( $\langle \lambda \rangle$ ) as a function of  $M_{\text{BH}}$  for several redshift ranges, scaled by  $\frac{1}{(1+z)^3}$ , with Poisson error bars [Note that the datapoints' x-positions for each z-bin have been shifted to the right (3% increase for each z-bin) such that the error bars are distinguishable]. We also show the typical host halo mass corresponding to the given BH mass on the top axis. *Filled circles*: Average gas density at the BHs position ( $\rho_{\text{BH}}$ ) for  $z = 4.75 - 5$ .

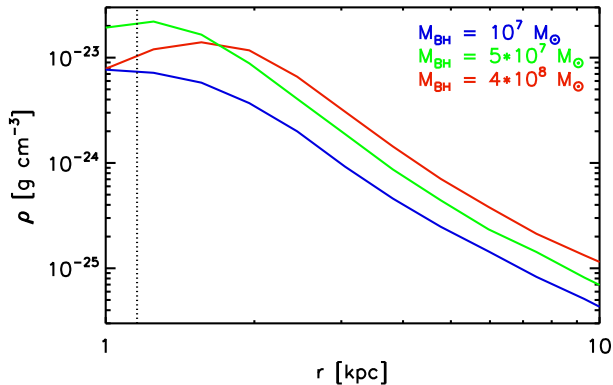


FIG. 2.— Gas density profiles averaged among 100 black holes with mass  $\sim 10^7 M_{\odot}$  (blue),  $\sim 5 \times 10^7 M_{\odot}$  (green),  $\sim 4 \times 10^8 M_{\odot}$  (red). Dotted line shows the gravitational softening length.

$M_{\text{BH}}$  in both magnitude and distance. This suppression of the local gas density is caused by the feedback of the black hole, with the stronger feedback of high-mass BHs producing the strongest effect (see Di Matteo et al. (2011) for detailed investigation of feedback among massive BHs).

We also show the typical mass of halos hosting a given  $M_{\text{BH}}$  on the top axis, noting that the Eddington ratio peaks at a host halo mass of  $\sim 7 \times 10^{11} - 1 \times 10^{12} M_{\odot}$ . This mass very closely matches the critical shock heating scale of  $\sim 6 \times 10^{11} M_{\odot}$  (Dekel & Birnboim 2006; Dekel et al. 2009, and consistent with our simulation), above which infalling gas is shock heated near the virial radius to the

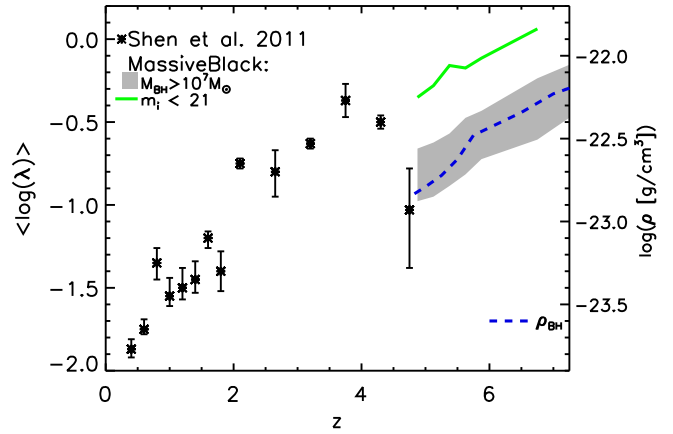


FIG. 3.— Redshift evolution of the Eddington ratio for black holes with  $M_{\text{BH}} > 10^7 M_{\odot}$  (shaded region shows 1- $\sigma$  standard deviation in  $\log(\lambda)$ ) and i-band magnitude  $m_i < 21$  (green line) compared with data from Shen & Kelly (2011) (black asterisks). We also show the evolution in the gas density around BHs for comparison (blue dashed line).

virial temperature of the halo. Dekel & Birnboim (2006) suggest that in these halos AGN feedback becomes more significant, since the dilute shock-heated gas will be more susceptible to heating and pushing by the central AGN. This would thus produce a suppression in the gas density profile, consistent with the picture described above and the downturn in Figure 1.

In addition to the evolution in  $\lambda$  with  $M_{\text{BH}}$ , Figure 1 also shows that  $\lambda$  evolves with redshift as  $\sim (1+z)^3$ , which is also caused by the evolution in the local gas density. In Figure 3 we show the evolution in  $\langle \log(\lambda) \rangle$  with redshift among  $M_{\text{BH}} > 10^7 M_{\odot}$  BHs (shaded region, showing 1- $\sigma$  standard deviation). We plot the average gas density at the BH (blue dashed line), showing the evolution in  $\lambda$  is primarily caused by the evolution in  $\rho_{\text{BH}}$  (recall  $M_{\text{BH}} \propto \rho_{\text{BH}}$ ). We also compare to observational measurements of Shen & Kelly (2011) (black asterisks), showing that this general redshift evolution is consistent with current observations, and the normalization is approximately consistent if we use a similar magnitude cut (i-band magnitude  $m_i < 21$  - green line).

### 3.2. Eddington Ratio Distributions

In addition to investigating the mean Eddington ratio, we also study the distribution of  $\lambda$  among comparable BHs. Previous work on the  $\lambda$ -distribution has often found roughly log-normal distributions using both observational (Kollmeier et al. 2006; Netzer et al. 2007; Netzer & Trakhtenbrot 2007; Willott et al. 2010; Trakhtenbrot et al. 2011) and phenomenological approaches (Shankar et al. 2011) [though Aird et al. (2011) find  $\lambda$  to follow a power law when selected for host stellar mass, rather than BH mass]. However, these observational studies necessarily incorporate several uncertainties, such as sample selection and scatter in black hole mass estimators, which we can bypass, using our simulation to probe our black holes' Eddington ratios directly. In Figure 4 we show the distribution of Eddington ratios among black holes selected by  $M_{\text{BH}}$  (black histograms). We find that the distribution produced by

our simulation is indeed log-normal, in keeping with observational findings (Kollmeier et al. 2006; Netzer et al. 2007; Netzer & Trakhtenbrot 2007; Willott et al. 2010; Trakhtenbrot et al. 2011). In particular, we note that the distribution remains log-normal regardless of the mass considered, with Figure 4 showing this holds among black holes that are below, at, and above the peak observed in Figure 1.

Because we find  $\lambda$  to follow a log-normal distribution and the mean of that distribution obeys a well-defined curve with  $M_{\text{BH}}$  (Figure 1), we are able to provide a general fitting formula for  $P(\lambda|M_{\text{BH}}, z)$ , the probability distribution of black hole Eddington ratios as a function of redshift and black hole mass:

$$P(\lambda|M_{\text{BH}}, z) = \frac{1}{\lambda\sigma_m\sqrt{2\pi}} e^{-\frac{(\ln(\lambda)-\mu_m)^2}{2\sigma_m^2}} \quad (1)$$

where  $\mu_m$  and  $\sigma_m$  are the mean and standard deviation of  $\ln(\lambda)$ , respectively, and are fit by  $\sigma_m \sim 0.39$  and

$$\mu_m = (1+z)^3 A e^{-\left(\log_{10}\left(\frac{M_{\text{BH}}}{M_\mu}\right)\right)^2/2\sigma_0^2}, \quad (2)$$

with  $A \sim .00094$ ,  $M_\mu = 5 \times 10^7 M_\odot$ , and  $\sigma_0 \sim 0.85$ . In Figure 4 we plot the distribution predicted by Equations 1&2 (red curve) compared the the actual distribution, showing that this simple formula is capable of reproducing the distribution of  $\lambda$  for BHs in our simulation across a wide range of masses and redshifts, without requiring knowledge of individual black hole environments.

In addition to the distribution for a mass-selected sample, in Figure 5 we show the Eddington ratio distribution from our simulation (red histogram) compared to the observed distribution from Kollmeier et al. (2006) (black histogram) for two luminosity selected samples. We again note that the distribution is described by a roughly log-normal distribution, and that our simulation is approximately consistent with observational results.

Furthermore, by combining  $P(\lambda|M_{\text{BH}}, z)$  with the black hole mass function ( $\Phi_{\text{BH}}$ ) we can obtain the Eddington ratio probability distribution for a luminosity-selected sample:

$$P(\lambda|L_{\text{BH}}, z) = \frac{\Phi_{\text{BH}}(M_{\text{BH}})P(\lambda|M_{\text{BH}}, z)}{\int_0^\infty \Phi_{\text{BH}}(M_{\text{BH}})P(\lambda|M_{\text{BH}}, z)d\lambda} \quad (3)$$

where  $M_{\text{BH}} = \frac{\sigma_\tau L_{\text{BH}}}{4\pi G m_p c \lambda}$ . In Figure 5 we plot this predicted probability distribution (using our simulation's mass function) in red, showing  $P(\lambda|L_{\text{BH}}, z)$  is well predicted in this manner. We note that this approach is significant as it provides a potentially powerful tool for constraining the black hole mass function using observations of the Eddington ratio distribution. We show this in Figure 5 by plotting  $P(\lambda|L_{\text{BH}}, z)$  based on three different local mass functions: the Shankar et al. (2009) mass function (dashed green); the Shankar et al. (2009) mass function derived from the Hopkins et al. (2007b) luminosity function (dashed blue), and the mass function of Hopkins et al. (2007a) (dashed pink). Because  $P(\lambda|L_{\text{BH}})$  is sensitive to the slope of  $\Phi_{\text{BH}}$ , the distribution of  $\lambda$  at high  $L_{\text{BH}}$  (where the mass function is steepest) varies substantially with the mass function used, suggesting that with improved statistics from upcoming surveys, we could use the observed  $P(\lambda|L_{\text{BH}})$  to constrain the slope

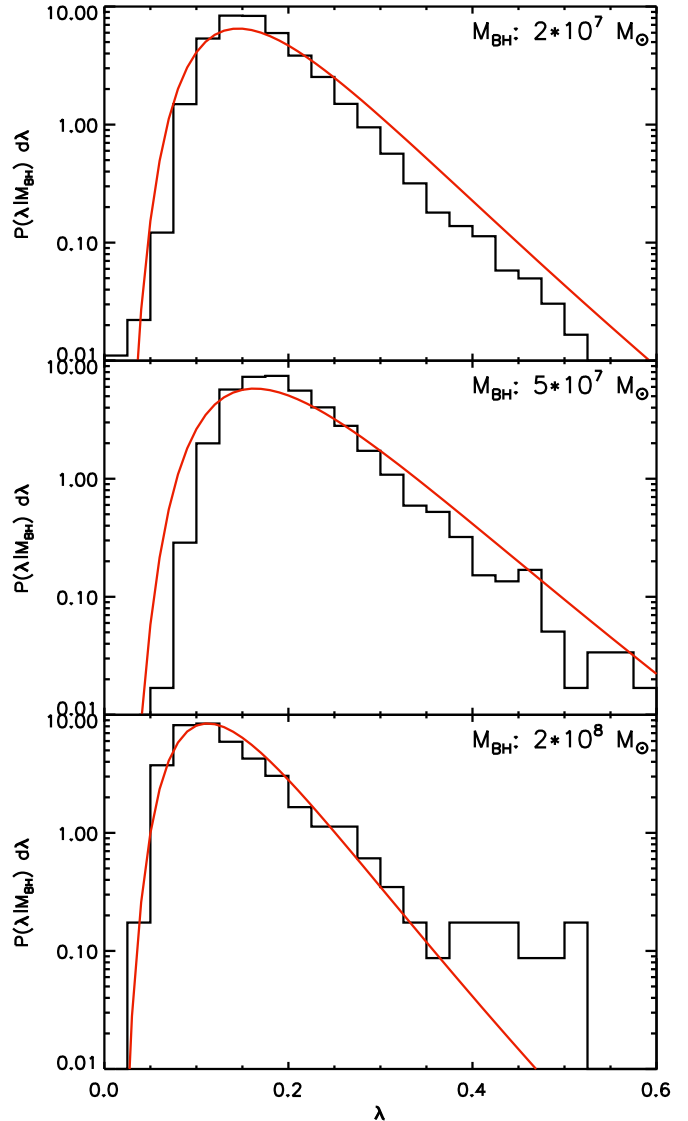


FIG. 4.— Eddington ratio distribution for black holes at three different mass scales (black) and the predicted distribution from Equations 1&2 (red curves).

of the black hole mass function at high redshift, even without measurements of the black hole masses.

#### 4. CONCLUSIONS

With a new large-scale simulation, we show that the growth of black holes tends to follow a typical growth pattern. In general, we find that black holes grow more rapidly at higher redshift than comparable black holes at lower redshift, characterized by  $\lambda \propto (1+z)^3$ . This scaling is caused by the redshift evolution in the gas density about the black holes, and is comparable to current observational data from Shen & Kelly (2011).

The typical Eddington ratio also scales with  $M_{\text{BH}}$  such that  $\lambda$  peaks at  $M_{\text{BH}} \sim 4 - 8 \times 10^7 M_\odot$  (typically found in halos of  $\sim 7 \times 10^{11} - 1 \times 10^{12} M_\odot$ ). This peak is caused by evolution in the density of the gas at halo centers that is available to fuel black hole growth. In general, more massive black holes are found in more massive halos with correspondingly higher gas densities, hence  $\lambda$  grows with  $M_{\text{BH}}$  for low masses. However, above  $M_{\text{BH}} \sim 5 \times 10^7 M_\odot$

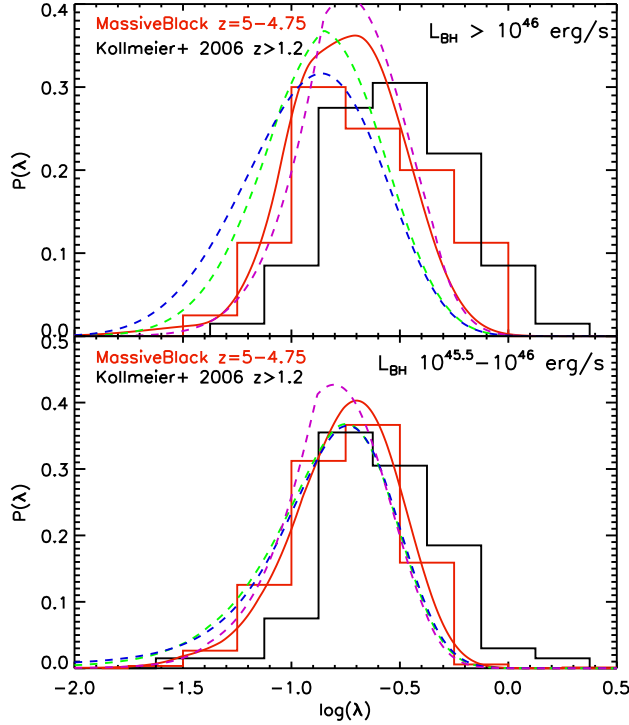


FIG. 5.— Distribution of Eddington ratios for BHs in our simulation (red histogram) compared with observational data from Kollmeier et al. (2006) (black histogram) for two luminosity bins. We also show the predicted distribution based on our fitting function (Equations 3) using our simulation’s mass function (solid red), the Shankar et al. (2009) base mass function (dashed green), the Shankar et al. (2009) mass function derived from the Hopkins et al. (2007b) luminosity function (dashed blue), and the mass function of Hopkins et al. (2007a) (dashed pink).

black hole feedback has a sufficiently strong effect on the local environment to suppress the density of the nearby gas. Thus although these more massive black holes are found in more massive halos with correspondingly higher gas densities in general, the feedback has significantly lessened the density of the innermost gas where accretion occurs. This suppression of the local gas density is stronger for more massive BHs, and causes  $\lambda$  to decrease for  $M_{\text{BH}} \gtrsim 5 \times 10^7 M_{\odot}$ .

Although the local environment is important for the accretion rate of individual black holes, we show that the distribution of Eddington ratios follows a roughly log-normal distribution regardless of the black hole population considered, consistent with current observational findings. We use this, together with the evolution in  $\langle \lambda \rangle$ , to provide a simple fitting formula for the distribution of Eddington ratio with  $(M_{\text{BH}}, z)$ . This general formula can be used for predicting the growth/evolution of black hole populations in theoretical and semi-analytic models (such as the evolution of the black hole mass function), for predicting the mass of observed high-redshift quasars, and, in conjunction with upcoming observations of the  $\lambda$ -distribution, to constrain the slope of the high-redshift black hole mass function.

#### ACKNOWLEDGMENTS

This work was supported by the National Science Foundation, NSF Petapps, OCI-0749212 and NSF AST-1009781. The simulations used in this paper were carried out on Kraken at the National Institute for Computational Sciences (<http://www.nics.tennessee.edu/>).

#### REFERENCES

- Aird J., et al., 2011, ArXiv e-prints  
 Begelman M. C., Volonteri M., Rees M. J., 2006, MNRAS, 370, 289  
 Booth C. M., Schaye J., 2009, MNRAS, 398, 53  
 Bower R. G., Benson A. J., Malbon R., Helly J. C., Frenk C. S., Baugh C. M., Cole S., Lacey C. G., 2006, MNRAS, 370, 645  
 Bromm V., Larson R. B., 2004, ARA&A, 42, 79  
 Bromm V., Loeb A., 2003, ApJ, 596, 34  
 Burkert A., Silk J., 2001, ApJ, 554, L151  
 Churazov E., Sazonov S., Sunyaev R., Forman W., Jones C., Böhringer H., 2005, MNRAS, 363, L91  
 Ciotti L., Ostriker J. P., 2007, ApJ, 665, 1038  
 Colberg J. M., di Matteo T., 2008, MNRAS, 387, 1163  
 DeGraf C., Di Matteo T., Khandai N., Croft R., Lopez J., Springel V., 2011, ArXiv e-prints  
 DeGraf C., Di Matteo T., Springel V., 2010, MNRAS, 402, 1927  
 Degraf C., Di Matteo T., Springel V., 2011, MNRAS, 413, 1383  
 Dekel A., Birnboim Y., 2006, MNRAS, 368, 2  
 Dekel A., et al., 2009, Nature, 457, 451  
 Di Matteo T., Colberg J., Springel V., Hernquist L., Sijacki D., 2008, ApJ, 676, 33  
 Di Matteo T., Khandai N., DeGraf C., Feng Y., Croft R., Lopez J., Springel V., 2011, ApJL submitted  
 Di Matteo T., Springel V., Hernquist L., 2005, Nature, 433, 604  
 Fan X., et al., 2006, AJ, 132, 117  
 Feng Y., et al., 2011, ArXiv e-prints  
 Ferrarese L., Merritt D., 2000, ApJ, 539, L9  
 Gebhardt K., et al., 2000, ApJ, 539, L13  
 Graham A. W., Driver S. P., 2007, ApJ, 655, 77  
 Hopkins P. F., Hernquist L., Cox T. J., Robertson B., Krause E., 2007a, ApJ, 669, 45  
 Hopkins P. F., Richards G. T., Hernquist L., 2007b, ApJ, 654, 731  
 Jiang L., et al., 2009, AJ, 138, 305  
 Johansson P. H., Naab T., Burkert A., 2008, Astronomische Nachrichten, 329, 956  
 Kollmeier J. A., et al., 2006, ApJ, 648, 128  
 Kormendy J., Richstone D., 1995, ARA&A, 33, 581  
 Lemson G., Virgo Consortium t., 2006, ArXiv Astrophysics e-prints: 0608019  
 Lopez J., Degraf C., DiMatteo T., Fu B., Fink E., Gibson G., 2011, in Statistical and Scientific Databases Management Conference (SSDBM), Portland, OR  
 Magorrian J., et al., 1998, AJ, 115, 2285  
 Mayer L., Kazantzidis S., Madau P., Colpi M., Quinn T., Wadsley J., 2007, Science, 316, 1874  
 Netzer H., Lira P., Trakhtenbrot B., Shemmer O., Cury I., 2007, ApJ, 671, 1256  
 Netzer H., Trakhtenbrot B., 2007, ApJ, 654, 754  
 Sazonov S. Y., Ostriker J. P., Sunyaev R. A., 2004, MNRAS, 347, 144  
 Shakura N. I., Sunyaev R. A., 1973, A&A, 24, 337  
 Shankar F., Weinberg D. H., Miralda-Escudé J., 2009, ApJ, 690, 20  
 Shankar F., Weinberg D. H., Miralda-Escudé J., 2011, ArXiv e-prints  
 Shen Y., Kelly B. C., 2011, ArXiv e-prints  
 Sijacki D., Springel V., di Matteo T., Hernquist L., 2007, MNRAS, 380, 877  
 Sijacki D., Springel V., Haehnelt M. G., 2009, MNRAS, 400, 100  
 Springel V., 2005, MNRAS, 364, 1105  
 Springel V., Di Matteo T., Hernquist L., 2005a, MNRAS, 361, 776  
 Springel V., Hernquist L., 2003, MNRAS, 339, 289  
 Springel V., et al., 2005b, Nature, 435, 629

Trakhtenbrot B., Netzer H., Lira P., Shemmer O., 2011, ApJ, 730,  
7  
Tremaine S., et al., 2002, ApJ, 574, 740

Willott C. J., et al., 2010, AJ, 140, 546  
Yoshida N., Omukai K., Hernquist L., Abel T., 2006, ApJ, 652, 6